PROCEEDINGS, 43rd Workshop on Geothermal Reservoir Engineering
Stanford University, Stanford, California, February 12-14, 2018
SGP-TR-213

Analytical and Numerical Modeling of Heat Transport in Fractured Reservoirs

Quanlin Zhou*, Curtis M. Oldenburg, Jonny Rutqvist, Timothy J. Kneafsey, and The EGS Collab Team

Energy Geosciences Division, Lawrence Berkeley National Laboratory, Berkeley, CA 94720

*Corresponding E-mail address: qzhou@lbl.gov

Keywords: Geothermal, heat transport, fractured rock, matrix, analytical solutions, numerical modeling

ABSTRACT

Modeling of thermal perturbations induced by injecting fluids of different temperature into deep fractured reservoirs is important for design and analysis of geothermal energy production including enhanced geothermal systems, and thermal energy storage. A novel analytical solution was first developed to couple global heat convection-conduction in fractures with heat conduction in the rock matrix and aquitards. This coupling was developed by using the unified-form diffusive flux equations recently developed for various shapes of matrix blocks and aquitards (Zhou et al., 2017a, b). A number of generic scenarios of flow regimes and system types were considered for a general study. We then used TOUGH2-MP/EOS1 to model the cold-water injection test planned for the sub-vertical hydraulic fracture at the EGS Collab test site. Our modeling results of water injection and heat transfer in the planned fracture of dimension 12 m × 10 m suggest that a measurable thermal breakthrough may not occur at the production well within the test period of 100 days. This infeasibility may be attributed to (1) small fracture aperture (i.e., 100 μm) and (2) high heat gain from the rock matrix with a thermal diffusivity of $D_m = 1.42 \times 10^{-6}$ m^2/s.

1. INTRODUCTION

Estimates of flow and heat transfer in fractures are needed for design and analysis of the EGS Collab experiments (Kneafsey et al., 2018). We first developed analytical solutions for modeling heat transport in general fractured reservoirs and used the developed analytical solutions to perform some sensitivity analysis to better understand the effect of rock properties, injection rate, and fracture aperture on thermal breakthrough. We then developed a TOUGH2-MP/EOS1 model for the hydraulic fracture of limited extent at the EGS Collab site, simulated the heat transport in the fracture and rock matrix, and performed the feasibility and design study on the injection rate and test duration for the thermal tests.

A large number of analytical solutions have been developed for heat transport in idealized aquifer-aquitard systems (e.g., Lauwerier, 1955; Avdonin, 1964; Chen and Reddell, 1983) and fracture-matrix systems (e.g., Bodvarsson and Tsang, 1982; Ascencio et al., 2014). These developments are based on (1) solving the heat conduction equation in the infinite or finite aquitard/slab, (2) calculating the heat flux at the aquifer-aquitard or fracture-matrix interface, and (3) solving the global heat transport equation for the aquifer/fracture, all in the Laplace domain. Analytical or numerical Laplace inversion are used to calculate the time-domain temperature solutions (de Hoog et al., 1982). These solutions are available for 1-D linear and radial fluid flow systems. The 1-D heat convection and conduction are considered in the aquifer/fracture and 1-D heat conduction in the direction normal to the aquifer/fracture is considered in the aquitard/slab. These solutions are specific to the system setup of an infinite aquifer/fracture and an infinite and finite aquitard/slab. In reality, a fractured reservoir may contain millions of connected discrete fractures of limited length and millions of matrix blocks of finite dimensions and shapes. In this study, we build on the long history of prior work to develop and apply analytical and numerical models to inform EGS Collab field testing.

To honor the nature of a fractured reservoir that may be overlain and underlain by aquitards, we developed a suite of analytical solutions using the concept of transfer function developed for linear transport systems (Danckwerts, 1953; Villermaux, 1987; Sardin et al., 1991). The global transfer function was used to represent the convection, convection-conduction, and convection-dispersion of heat in the fracture network, while the local transfer function was used to represent the heat flux at the fracture-matrix interfaces. Both transfer functions were developed independently, and the final solutions were developed by plugging the local transfer function into the global one in the Laplace domain. The local transfer function was based on the unified-form diffusive flux equation recently developed for regular matrix blocks (e.g., cylinders, spheres, slabs, squares, cubes, rectangles, rectangular parallelepipeds) by Zhou et al. (2017a, b).

2. ANALYTICAL SOLUTIONS OF HEAT TRANSPORT

2.1 Procedure of Solution Development

We developed a suite of analytical solutions using the concept of transfer function developed for linear transport systems (Danckwerts, 1953; Villermaux, 1987; Sardin et al., 1991). The global transfer functions, $G(x,t)$, and their Laplace transforms, $G^*(x,s)$, are used to solve the heat transport equation for the fracture network or aquifer, where x, t, s are the 1-D coordinate, the time, and the Laplace variable, respectively. The solutions of $G^*(x,s)$ for 1-D linear and radial heat convection without the coupling with aquitard/matrix block are denoted as $G_0^*(x,s)$ and available in the literature (e.g., Tang et al., 1981; Moench and Ogata, 1981). The local transfer function, $g(t)$, and its Laplace transfer, $g^*(s)$, represent the conductive heat flux through fracture-matrix/aquifer-aquitard interfaces. The local transfer function is often referred to as the memory function (Villermaux, 1987; Carrera et al., 1998; Haggerty et al., 2000; Dentz and Berkowitz, 2003) in the solute transport community. The final solution for the aquifer-aquitard and fracture-matrix systems is $G^*(x,s) =$

$G_0^*(x, s[1+g^*(s)])$ by using $s \Rightarrow s[1+g^*(s)]$. This procedure of solution development is completely different from the step-by-step derivation one that has been used solely in the heat transport community.

Our solution procedure allows for any analytical representations of the memory function $g^*(s)$, thus relaxing the constraints of existing analytical solutions on the geometry of the matrix blocks. A representative elementary volume (REV) of a fractured medium can consist of either uniform matrix blocks with a regular shape (e.g., cylinder, sphere, slab, square, cube, rectangle, rectangular parallelepiped) and size, or a mixture of matrix blocks of different shapes and sizes (see Figure 1). For the system in Figure 1, the memory function can be developed easily for the combined effect of the mixture of matrix blocks and the aquitards. The memory function $g^*(s)$ was derived using the unified-form diffusive flux equation recently developed for regular shapes of matrix blocks by Zhou et al. (2017a, b).

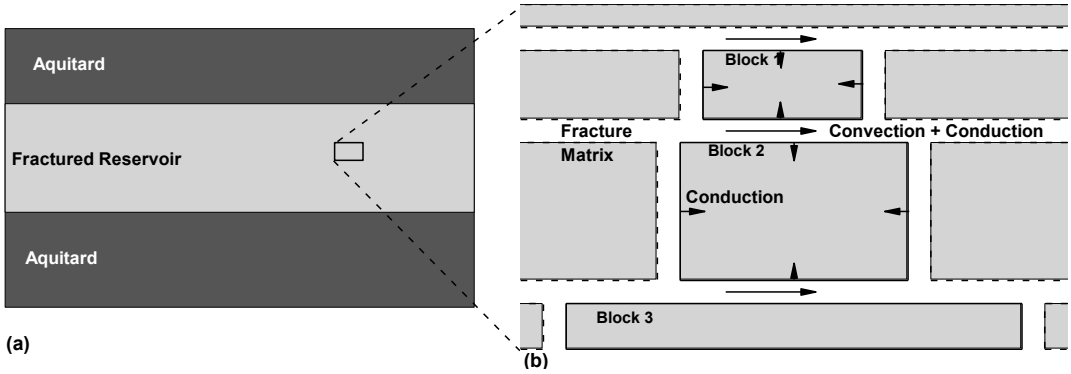

Figure 1. (a) A fractured reservoir overlain and underlain by aquitards, and (b) a portion of REV consisting of fractures and matrix blocks of different shapes and sizes, as well as heat convection-conduction in fractures coupled with heat conduction in matrix blocks.

2.2 Block-Scale Solutions

2.2.1 Temperature Solutions

The heat conduction equation for a matrix block can be written

$$\frac{\partial T_d}{\partial t} = -D_m \nabla \cdot \nabla T_d, \tag{1}$$

where T_d is the dimensionless temperature of the matrix block with a constant, unit fracture temperature change and zero initial matrix temperature, and D_m is the thermal diffusivity, and t is the time.

For a 3-D rectangular parallelepiped with three coordinates x_i $(i = 1, 2, 3)$, we introduce the dimensionless spatial variables and the dimensionless times

$$x_{di} = x_i/l_i\,, t_{di} = D_m t/l_i^2 = R_{li}^2 t_d, \tag{2a}$$

where the fracture half-spacing l_i, the aspect ratio R_{li}, and the dimensionless area-to-volume ratio R are defined by

$$l = l_1 \leq\ l_2 \leq\ l_3, R_{li} = l/l_i, R = Al/V \tag{2b}$$

where A, V and l are the boundary area, volume, and minimum half-width of the blocks. Note that $t_d = Dt/l^2$ is always written in terms of the minimum half-width. The same definitions hold for 2-D rectangular blocks.

It is well-known that the dimensionless temperature solution for a 1-D slab, a 2-D rectangle, and a 3-D rectangular parallelepiped can be written in a general product form (Crank, 1975)

$$T_d = 1 - \prod_{i=1}^{N_d} T'_{di}(x_{di}, t_{di}) \tag{3a}$$

where N_d is the dimensionality of the blocks (= 1 for slabs, = 2 for rectangles, = 3 for rectangular parallelepipeds), and $T'_{di}(x_{di}, t_{di})$ is the 1-D slab temperature solution for the case with a unit initial temperature and zero boundary temperature, which is complementary to the T_d solution $T'_{di}(x_{di}, t_{di}) = 1 - T_{di}(x_{di}, t_{di})$.

For numerical evaluation, we first consider the 1-D slab complementary solution in each direction independently, and then calculate the early- and late-time solutions in that direction using time partitioning with its own dimensionless time (t_{di}) and the same switchover dimensionless time t_{d0}^T $(= 0.27)$ for slabs as follows (Zhou et al., 2017b):

$$T'_{di}(x_{di}, t_{di}) = \begin{cases} 1 - \left[\operatorname{erfc}\frac{1-x_{di}}{2\sqrt{t_{di}}} + \operatorname{erfc}\frac{1+x_{di}}{2\sqrt{t_{di}}}\right], & t_{di} < t_{d0}^{T} \quad (3b) \\ \frac{4}{\pi}\exp\left[-\frac{\pi^2 t_{di}}{4}\right]\cos\left(\frac{1}{2}\pi x_{di}\right), & t_{di} \geq t_{d0}^{T} \quad (3c) \end{cases}$$

We finally perform the multiplication of the calculated solutions for all the directions using (3a). The errors of the approximation solution in comparison with the exact exponential-series solutions or the exact error-function-series solutions are less than 0.3%.

Figure 2 shows the contours of dimensionless temperature calculated using the developed approximate solutions for six rectangular blocks over the spatial domain at three selected times ($t_d = 0.02, 0.2,$ and 0.5). Three rectangles with aspect ratios $R_{l2} = 1.0, 0.5, 0.2$ and three rectangular parallelepipeds with three pairs of aspect ratios $(R_{l2},\ R_{l3}) = (1.0,\ 1.0), (0.5,\ 0.2), (0.2,\ 0.1)$ are used. The grids for calculating dimensionless temperature have 201 logarithmically spaced dimensionless times in the range $t_d = [10^{-6}, 10]$ and 201 linearly spaced spatial variables $x_{di} = [0, 1]$. Figures 2a-c shows the contours of dimensionless temperature at three different times for three rectangles with $R_{l2} = 1.0, 0.5, 0.2$, respectively. At $t_d = 0.02$, the profile of T_d from the fixed-temperature boundary to the temperature front looks like that for a slab, except at the rectangular corner. At later time, the temperature over the entire domain is affected by the temperature profiles in different directions. The highly anisotropic rectangle with $R_{l2} = 0.2$ acts like a slab more than the isotropic square. Clearly, the aspect ratio has a significant effect on the temperature distributions. As shown in Figures 2d-f, the aspect ratio in the third dimension also affects the temperature solution significantly at all of the three times. This indicates that heat conduction in 2-D/3-D rectangular blocks cannot be approximated using that in 1-D slabs.

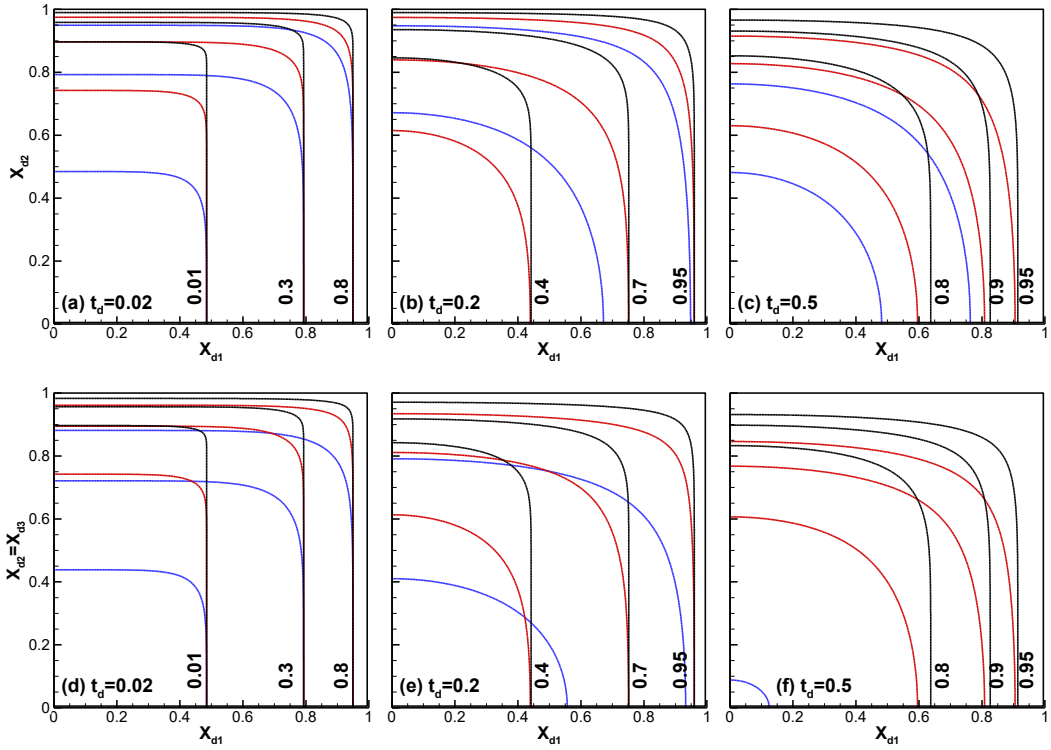

Figure 2. (a-c) Contour of dimensionless temperature (T_d) over the 2D rectangles (x_{d1}, x_{d2}) at $t_d = 0.02, 0.2, 0.5$, and (d-f) over 3D rectangular parallelepipeds (x_{d1}, x_{d2}) with $x_{d3} = x_{d2}$ at $t_d = 0.02, 0.2, 0.5$. Note that the contour lines and their labels for the three rectangles with $R_{l2} = 1.0$ (in blue lines), 0.5 (in red), and 0.2 (in black) and the three parallelepipeds with $(R_{l2}, R_{l3}) = (1.0, 1.0)$ (in blue), (0.5, 0.2) (in red), and (0.2, 0.1) (in black).

The temperature solution in 1-D slabs, 2-D rectangles, and 3-D rectangular parallelepipeds can be easily calculated using equation (3) with high computational efficiency and accuracy. These solutions can support the refinement of numerical schemes (e.g., dual-porosity and multiple interacting continuum (MINC) models), without the need of high-resolution numerical modeling (Pruess and Narasimhan, 1985; Lim and Aziz, 1995).

2.2.2 Fracture-Matrix Diffusive Flux Equation

The unified-form, dimensionless transient heat flux can be written (Zhou et al., 2017a, b):

$$f_d = \begin{cases} a_1/\left(2\sqrt{t_d}\right) + a_2 + \frac{3}{2}a_3\sqrt{t_d}, & t_d < t_{d0} \\ \sum_{j=1}^{N} b_{1j} b_{2j} \exp\left(-b_{2j} t_d\right), & t_d \geq t_{d0} \end{cases} \tag{4}$$

where t_{d0} is the switchover dimensionless time for diffusive flux, $a_1, a_2,$ and a_3 are the parameters for the early-time solution, and $b_{1j}, b_{2j},$ and N are the parameters for the late-time exponential solution. For a rectangular parallelepiped, these solution parameters are

$$a_1 = 2(1 + R_{l2} + R_{l3})/\sqrt{\pi},\ \ a_2 = -4(R_{l2} + R_{l3} + R_{l2}R_{l3})/\pi,\ \ a_3 = 8R_{l2}R_{l3}/\pi^{3/2} \tag{5a}$$

$$b_{1j} = \left(\frac{8}{\pi^2}\right)^3 / \left[(2n_{1j} - 1)^2 (2n_{2j} - 1)^2 (2n_{3j} - 1)^2\right] \tag{5b}$$

$$b_{2j} = \frac{\pi^2}{4} c_j;\ c_j = \left((2n_{1j} - 1)^2 + \left(2n_{2j} - 1\right)^2 R_{l2}^2 + \left(2n_{3j} - 1\right)^2 R_{l3}^2\right) \tag{5c}$$

For both 2-D and 3-D rectangular blocks, the number of exponential terms (N) needed for the late-time solutions can be determined practically using

$$c_j \leq 11 \text{ with } b_{1j} \exp\left(-b_{2j} t_{d0}\right) \geq tol \tag{5d}$$

Figure 3 shows the calculated dimensionless transient heat flux for the same three rectangles and rectangular parallelepipeds, as well as a slab.

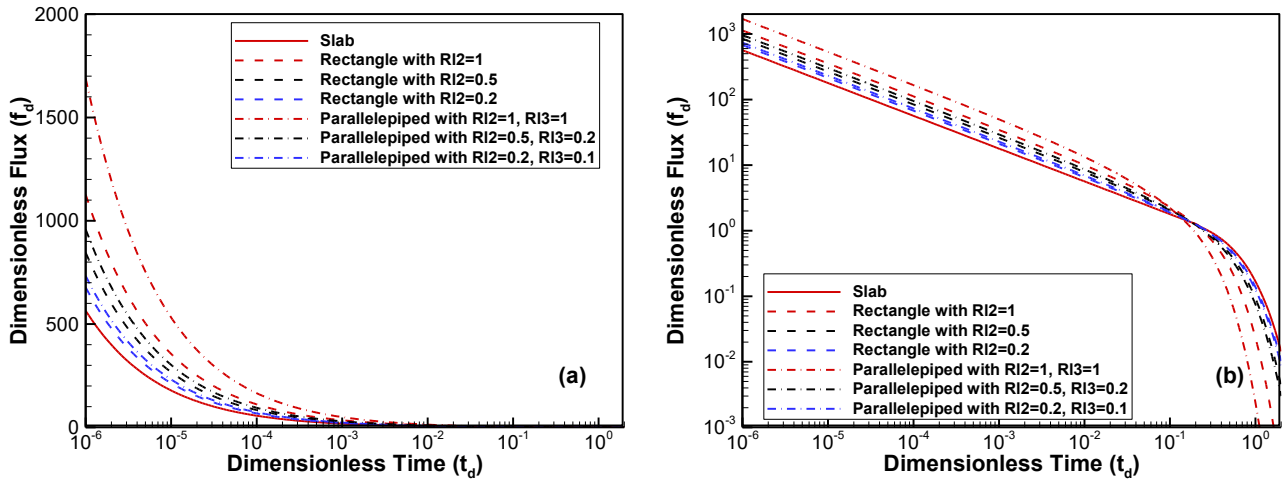

Figure 3. Dimensionless transient flux (f_d) calculated using the combined solutions with time partitioning for 1-D slab-like and 2-D/3-D rectangular blocks with different aspect ratios. Note that (a) is in the log-linear scale and (b) is in the log-log scale.

3. NUMERICAL MODELING OF THERMAL TESTS AT THE EGS COLLAB SITE

At the EGS Collab site, thermal tests are planned for characterizing the heat transfer properties of the stimulated fracture and the rock matrix (Kneafsey et al., 2018). In these planned tests, cold water will be injected into the fracture through the injection well, and water production will be performed at the production well to form a dipole system. The stimulation modeling shows that the hydraulic fracture is either a linear fracture of 12 m × 10 m with the influence of the zero stress in the drift or a radial fracture of radius of 20 m centered at the stimulation/injection well. No analytical solutions are available for heat transport because of the limited extent of the fracture. Numerical simulations were conducted using TOUGH2-MP/EOS1 (Pruess et al., 2012; Zhang et al., 2008). The main objective of these simulations was to show the feasibility of thermal breakthrough at the production well within a reasonable test time. The well spacing is 10 m. The 3-D numerical mesh is shown in Figure 4 and the rock properties in the baseline case and sensitivity-analysis cases, as well as the water injection rate and temperature, are listed in Table 1.

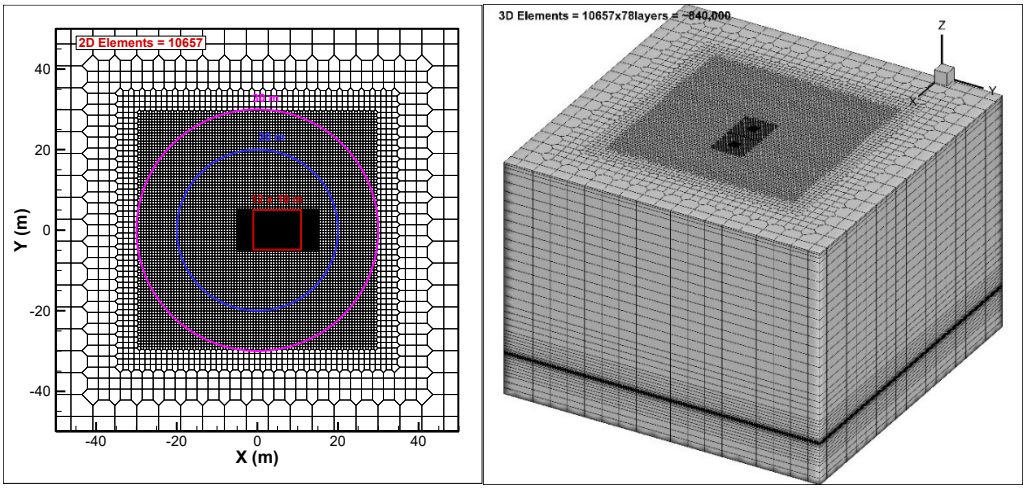

Figure 4. 2-D irregular mesh template with 10,657 elements (left-hand side) with three fracture cases: a radial fracture with a radius of 20 m (in blue) or 30 m (in pink) around the injection/stimulation well and a linear fracture with 12 m × 10 m (in red). On the right-hand side we show the 3-D irregular mesh of ~830,000 elements formed by stacking 78 layers of the template along with local refinement around the fracture which is shown horizontal in this figure. Note that the actual fracture is expected to be vertical and the injection and production wells are horizontal.

Table 1. Baseline and sensitivity values of fracture and matrix properties and injection parameters for the thermal-test modeling

Rock Properties	Baseline Value	Sensitivity Values
Matrix permeability	0.20×10^{-18} m^2 or 0.2 μD	
Matrix porosity	0.003 (Oldenburg et al., 2016, p29)	
Matrix thermal conductivity (K_m)	3 W/m°C	1, 0.3, 0.1, 0.01 W/m°C
Grain density	2730 kg/m^3	
Grain specific heat	775 J/kg°C	
Fracture permeability	830×10^{-12} m^2 or 830 D	
Fracture porosity	1	
Fracture water thermal conductivity	0.615 W/m°C	
water density	995.7 kg/m^3	
water specific heat	4178 J/kg°C	
Fracture aperture	100 μm	
Injection rate (Q)	400 ml/min	4,000 ml/min
Initial rock temperature	35 °C	
Injection temperature	5 °C	

As shown in Figure 5a, matrix thermal conductivity in the range between 1 and 3 W/m°C does not affect the temperature breakthrough curve (BTC) at the production well, but a further reduction in the matrix thermal conductivity will significantly affect the temperature BTC. This indicates that the uncertainty that we have in thermal conductivity of the rock at the EGS Collab site will not impact our interpretation of thermal breakthrough when the thermal breakthrough occurs with a negligible temperature change. Figure 5b shows the profiles of temperature at different distances away from the injection well in the baseline case. The heat gain from the rock matrix in comparison with thermal convection in the fracture increases with the distance from the injection well. This results in delayed arrival time of the thermal front with attenuated temperature change at distance farther away from the injection well. At the production well, the fluid temperature decreases by just 0.2 °C at 100 days. The delayed temperature arrival with attenuated temperature change can be attributed to (1) the heat gain from the rock matrix with high thermal diffusivity that is much higher than matrix tracer diffusivity, and (2) small fracture aperture of 100 μm.

It appears that thermal tests at an injection rate of 400 ml/min are not feasible for generating measurable thermal breakthrough at the production well because of high matrix thermal diffusivity ($D_m = 1.42 \times 10^{-6}$ m^2/s) and associated thermal interaction with the rock matrix. Sensitivity studies show thermal breakthrough is possible only for $D_m = 4.3 \times 10^{-8}$ m^2/s with a matrix thermal conductivity of 0.01 W/m°C. This indicates that multitracer tests with different injection rates and diffusivity may be suitable for assessing the heat-transfer performance and effective heat transfer area. The thermal tests are feasible at the production well only with a higher injection rate (4,000 ml/min, see Figure 5a) or locally at the injection well by monitoring cooling-induced changes in fracture aperture using the SIMFIT tool specifically designed for the EGS Collab project. In the latter, the injection time can be short and the cooling-induced aperture change can be local near the injection well.

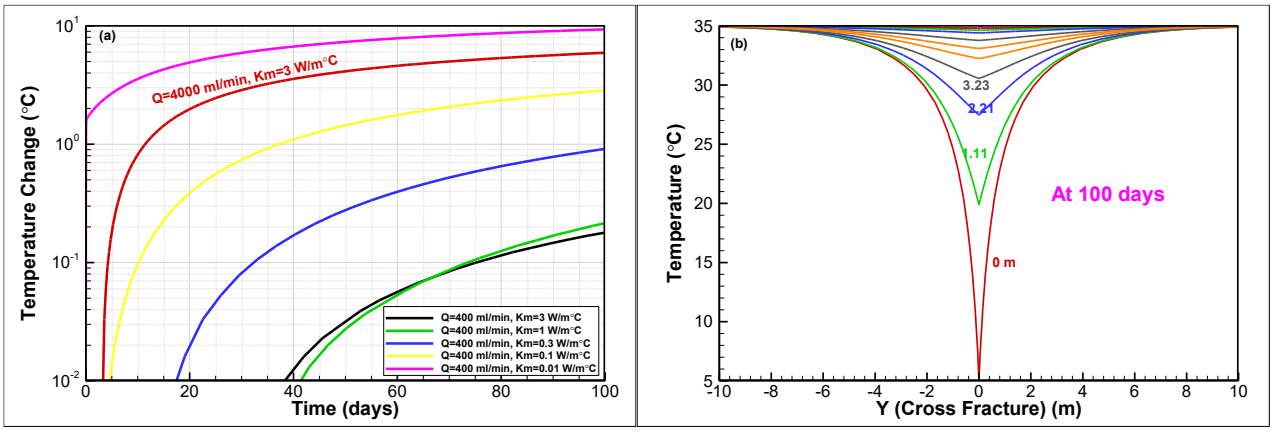

Figure 5. (a) Thermal breakthrough curves for the baseline and reduced wet matrix thermal conductivity and increased injection rate, while all other parameters are kept at their baseline values (left-hand side), and (b) baseline profiles of temperature in the fracture and rock matrix at different distances from the injection well.

4. CONCLUSIONS

A fractured reservoir may contain millions of connected discrete fractures of limited length and millions of matrix blocks of finite dimensions and shapes. This fractured reservoir may be idealized by assuming (1) 1-D linear or radial fluid flow in the network of uniform-aperture fractures, and (2) a mixture of matrix blocks with regular shapes (e.g., cylinder, sphere, slab, square, cube, rectangle, rectangular parallelepiped) and different sizes in a representative elementary volume (REV) of the fractured medium. In this case, novel analytical solutions were developed to couple global heat convection-conduction in fractures with heat conduction in the rock matrix. Using the concept of transfer functions, we combined (1) the global transfer function for heat convection, convection-conduction, and convection-dispersion in the fracture network and (2) the local transfer function (i.e., memory function) using the unified-form diffusive flux equations recently developed for various shapes of matrix blocks and aquitards (Zhou et al., 2017a, b). A number of generic scenarios of flow regimes and system types was considered and presented.

For the EGS Collab test site, the planned sub-vertical hydraulic fracture is of a limited extent, radial or linear, and no analytical solutions are available. A TOUGH2-MP/EOS1 model was developed and run with the site-specific rock properties and injection rate. The modeling results for the linear fracture of 12 m × 10 m show that the thermal tests may not produce measurable thermal breakthrough at the production well within the test period of 100 days. This infeasibility may be attributed to (1) small fracture aperture (i.e., 100 μm) and high heat gain from the rock matrix with a thermal diffusivity of $D_m = 1.42 \times 10^{-6}$ m^2/s. The infeasibility may be mitigated by using a higher injection rate (i.e., 4 L/min) or focusing on the cooling-induced aperture change near the injection well that can be tracked using the SIMFIT tool.

ACKNOWLEDGMENTS

This material was based upon work supported by the U.S. Department of Energy, Office of Energy Efficiency and Renewable Energy (EERE), Office of Technology Development, Geothermal Technologies Office, under Award Number DE-AC02-05CH11231 with LBNL. The United States Government retains, and the publisher, by accepting the article for publication, acknowledges that the United States Government retains a non-exclusive, paid-up, irrevocable, world-wide license to publish or reproduce the published form of this manuscript, or allow others to do so, for United States Government purposes. This work was also supported by the California Energy Commission (CEC) through an Electric Program Investment Charge (EPIC) funding award on geothermal energy to LBNL under agreement EPC-16-022.

REFERENCES

Ascencio, F., Samaniego, F., and Rivera, J.: A heat loss analytical model for the thermal front displacement in naturally fractured reservoirs, *Geothermics*, **50**, (2014), 112–121.

Avdonin, N.A.: Some formulas for calculating the temperature field of a stratum subject to thermal injection, *Neft'i Gaz* (in Russian), **7**(3), (1964), 37.

Bodvarsson, G.S., and Tsang, C.F.: Injection and thermal breakthrough in fractured geothermal reservoirs, *Journal of Geophysical Research: Solid Earth*, **87**(B2), (1982), 1031–1048.

Carrera, J., Sanchez-Vila, X., Benet, I., Medina, A., Galarza, G., and Guimera, J.: On matrix diffusion: Formulations, solution methods and qualitative effects, *Hydrogeology Journal*, **6**(1), (1998), 178–190

Chen, C.S., and Reddell, D.L.: Temperature distribution around a well during thermal injection and a graphical technique for evaluating aquifer thermal properties, *Water Resources Research*, **19**(2), (1983), 351–363.

Crank, J.: The mathematics of diffusion (2nd ed.). New York, NY: Oxford University Press, (1975).

Danckwerts, P.V.: Continuous flow systems: Distribution of residence times, *Chemical Engineering Science*, **2**(1), (1953), 1-13.

de Hoog, F.R., Knight, J.H., and Stokes, A.N.: An improved method for numerical inversion of Laplace transforms, *SIAM Journal on Scientific and Statistical Computing*, **3**(3), (1982), 357–366.

Dentz, M., and Berkowitz, B.: Transport behavior of a passive solute in continuous time random walks and multirate mass transfer, *Water Resources Research*, **39**(5), (2003), 1111, doi:10.1029/2001WR001163.

Haggerty, R., McKenna, S.A., and Meigs, L.C.: On the late-time behavior of tracer test breakthrough curves, *Water Resources Research*, **36**(12), (2000), 3467–3479. https://doi.org/10.1029/2000WR900214

Kneafsey, T.J., Dobson, P., Blankenship, D., Morris, J., Knox, H., Schwering, P., White, M., Doe, T., Roggenthen, W., Mattson, E., Podgorney, R., Johnson, T., Ajo-Franklin, J., Valladao, C., and the EGS Collab team: An overview of the EGS Collab project: Field validation of coupled process modeling of fracturing and fluid Flow at the Sanford Underground Research Facility, Lead, SD, *PROCEEDINGS,* the 43rd Workshop on Geothermal Reservoir Engineering, Stanford University, Stanford, California, February 12-14, 2018, SGP-TR-213.

Lauwerier, H.A.: The transport of heat in an oil layer caused by the injection of hot fluid, *Applied Scientific Research*, Section A, **5**(2–3), (1955), 145–150.

Lim, K.T., and Aziz, K.: Matrix-fracture transfer shape factors for dual-porosity simulators, *Journal of Petroleum Science and Engineering*, **13**, (1995), 169–178.

Moench, A.F., and Ogata, A.: A numerical inversion of the Laplace transform solution to radial dispersion in a porous medium, *Water Resources Research*, **17**(1), (1981), 250-252.

Oldenburg, C.M., Dobson, P.F., Wu, Y., Cook, P., Kneafsey, T.J., et. al.: Intermediate-Scale Hydraulic Fracturing in a Deep Mine, kISMET Project Summary 2016, Lawrence Berkeley National Laboratory, LBNL-1006444, Berkeley, CA, (2016).

Pruess, K., and Narasimhan, T.N.: A practical method for modeling fluid and heat flow in fractured porous media, *Society of Petroleum Engineers Journal*, **25**(1), (1985), 14–26.

Pruess K, Oldenburg C.M., and Moridis G.: TOUGH2 user's guide, Report LBNL-43134, Lawrence Berkeley National Laboratory, Berkeley, CA, USA (2012).

Sardin, M., Schweich, M., Leij, F.J., and van Genuchten, M.T.: Modeling the nonequilibrium transport of linearly interacting solutes in porous media: A Review, *Water Resources Research*, **27**(9), (1991), 2287-2307.

Tang, D.H., Frind, E.O., and Sudicky, E.A.: Contaminant transport in fractured porous media: analytical solution for a single fracture, *Water Resources Research*, **17**(3), (1981), 555–564.

Villermaux, J.: Chemical engineering approach to dynamic modeling of linear chromatography: A simple method for representing complex phenomena from simple concepts, *Journal of Chromatography*, **406**, (1987) 11–26.

Zhang, K., Wu, Y.S., and Pruess, K.: User's guide for TOUGH2-MP—A massively parallel version of the TOUGH2 code, Report LBNL-315E. Lawrence Berkeley National Laboratory, Berkeley, CA, USA, (2008).

Zhou, Q., Oldenburg, C.M., Spangler, L.H., and Birkholzer, J.T.: Approximate solutions for diffusive fracture-matrix transfer: Application to storage of dissolved CO_2 in fractured rocks, *Water Resources Research*, **53**, (2017a), 1746–1762.

Zhou, Q., Oldenburg, C.M., Rutqvist, J., and Birkholzer, J.T.: Revisiting the fundamental analytical solutions of heat and mass transfer: The kernel of multirate and multidimensional diffusion, *Water Resources Research*, **53**, (2017b), 9960–9979.